RF Performance of Single Sideband Modulation Versus Dual Sideband Modulation in a Photonic Link

Preetpaul S. Devgan, *Senior Member, IEEE*, Dean P. Brown, *Member, OSA*, and Robert L. Nelson

***Abstract*—Single sideband optical modulation can be used in multiple RF photonic link applications. However, single sideband optical modulation is often thought to provide lower RF output power than traditional dual sideband modulation techniques. While true in one specific case, it is not true in all cases. We theoretically and experimentally analyze the RF performance of a photonic link utilizing a Z-cut dual-electrode Mach–Zehnder intensity modulator with a 90° RF hybrid that produces optical single sideband modulation. The single sideband performance is compared to double sideband modulation using the same Mach–Zehnder modulator in either a push–pull configuration using a 180° RF hybrid or a single-arm drive configuration. The optical sideband powers, RF output power and the output intercept power and spur-free dynamic range of the third-order intermodulation nonlinearity are compared both theoretically and experimentally for each of the three cases. The performance of a double sideband modulated link using an X-cut inherently push–pull Mach–Zehnder modulator is also compared theoretically, assuming the same V_π and insertion loss as the dual-electrode Mach–Zehnder modulator.**

***Index Terms*—Mach Zehnder modulator, RF photonics, single sideband optical modulation.**

I. Introduction

THE use of RF photonic links has grown significantly, especially in microwave frequency applications such as antenna remoting [1], delay lines [2], clock recovery [3], [4], RF generation with low phase noise [5], [6], and frequency discrimination of low power RF signals [7], [8]. The use of photonic techniques provides multiple benefits, including low loss, immunity to electromagnetic interference, and broad instantaneous bandwidths. The most commonly used links incorporate a Mach-Zehnder intensity modulator (MZM) to impose the RF signal onto the optical carrier. One of the advantages of using the MZM is being able to operate at the quadrature bias point, which adds no even-order distortion to the signal upon detection at the photodiode (PD) at the output of the link [9]. However, the MZM output results in dual sideband (DSB) optical modulation, which can be adversely affected by chromatic dispersion, resulting in RF fading [10] and added distortion [11].

Manuscript received August 1, 2014; revised November 13, 2014, December 10, 2014, and December 22, 2014; accepted December 23, 2014. Date of publication December 30, 2014; date of current version March 13, 2015.

P. S. Devgan is with the Air Force Research Laboratory, Sensors Directorate, WPAFB, Dayton, OH 45433 USA (e-mail: preetpaul.devgan@us.af.mil).

D. P. Brown is with UES, Inc., Dayton, OH 45432 USA (e-mail: dean.brown@osamember.org).

R. L. Nelson is with the Air Force Research Laboratory, Materials and Manufacturing Directorate, WPAFB, Dayton, OH 45433 USA (e-mail: robert.nelson.21@us.af.mil).

Color versions of one or more of the figures in this paper are available online at http://ieeexplore.ieee.org.

Digital Object Identifier 10.1109/JLT.2014.2387011

Single sideband (SSB) optical modulation has been shown to overcome the penalties due to chromatic dispersion effects [12]. SSB optical signals have been produced by multiple methods, including optical filtering of DSB modulation [13], using a 90° RF hybrid with a single push-pull MZM [14] and using a single electrode MZM with bi-directional optical inputs [15]. The use of SSB modulation in RF applications has grown, seeing use in optoelectronic oscillators [16] and to improve the linearity of both second [17] and third [18] order nonlinearities in PDs.

Despite the benefits of using SSB modulation, the use of SSB modulated RF photonic links continues to lag the traditional DSB modulation links. A previous study on RF photonic links has compared external modulation versus directly modulated links and encouraged the use of MZMs for these applications [19]. Along similar lines, this paper seeks to compare the use of different modulation formats and encourage the use of SSB modulated links. For example, one common misconception held by those who design RF photonic links is the RF output power of a SSB modulated photonic link is less than the DSB link, as there is only one sideband to beat with the optical carrier. While true for one specific case, it is not true for all DSB optical modulation links. It is also believed that since the RF output power is lower, the SFDR will be lower as well. Again this is not the case. This result may be obvious to those who design MZM components, but it is not obvious to the RF photonic link developers. Thus a comprehensive study that includes both theory and experimental validation is required.

In this paper we present a theoretical and experimental comparison of a SSB modulated link to a few different DSB modulated links. This paper addresses a gap in RF photonic link design that has limited the use of SSB modulated links to niche applications. Currently there are no detailed comparative studies of the optical sideband power, RF output power and third order nonlinear performance of an SSB modulated link and three other DSB modulated links. We start from the first principles of the MZM transfer function and derive analytic expressions for the different SSB and DSB cases. We then use the same dual electrode MZM to experimentally validate our theory. By using a dual electrode MZM that can be configured for different modulation formats we eliminate discrepancies that arise from having a different V_π and insertion loss that occur when using different MZMs. In our theoretical comparison to a DSB X-cut MZM, we assume that the X-cut MZM has the same V_π and insertion loss as the dual electrode MZM we are using. By using a high resolution OSA, we directly measure the optical sidebands of the different modulations and show the optical power changes between the different modulation formats, as well as the extinction of the SSB case. This measurement is done at an

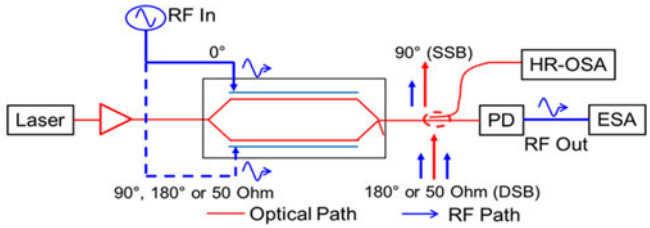

Fig. 1. Experimental setup for comparing single optical sideband and dual optical sideband modulated RF signals. HR-OSA: High resolution optical spectrum analyzer, PD: photodiode, ESA: electrical spectrum analyzer.

RF frequency that would not be observable on most OSAs. Our results will demonstrate that the RF output power for one of the DSB links is indeed 3 dB higher than the SSB link. However for the other two DSB links, the SSB link has the same RF output power. In addition, the output intercept power of the third order intermodulation nonlinearity is the same for a SSB modulated link when compared to three different DSB links, while still maintaining the quadrature bias condition of no-added even order nonlinearity. The results show the use of SSB modulated links provide no loss of RF performance when compared to most other DSB modulated links.

II. Theory and Experiment for Optical Power of SSB and DSB Modulation

In order to compare the SSB link with the DSB link, we will use the same Z-cut $LiNbO_3$ MZM that can be operated in both a push-pull and single arm RF drive configuration. As seen in Fig. 1, the MZM link consists of a CW laser source, whose output is connected to the MZM. The RF inputs of the MZM are connected to the RF signal source. In order to compare SSB to DSB modulation, the RF signal is either connected to a 90° hybrid (SSB), 180° hybrid (DSB) or just one of the RF inputs (DSB), with the other input connected to a 50 Ω load. The optical output of the MZM is then split, with a part of the modulated light sent to a high resolution optical spectrum analyzer (HR-OSA). The HR-OSA is used to record both the power levels of the sidebands as well as the carrier. The other part of the output is sent to a photodetector to recover the RF signal. The signal is then captured on an electrical spectrum analyzer in order to measure both the gain and the third order intermodulation product.

Starting from a previous analysis using a single MZM [9], the field amplitude at the input of the MZM can be related to the average optical power from the laser by $E_{\rm in}^{*}E_{\rm in} = 2\kappa_{\rm laser}^{2}P_{\rm laser}$, with $\kappa_{\rm laser}^{2} = Z_o/nA_{\rm eff}$, $Z_{\rm o}$ is the free space impedance of 377 Ω, n is the refractive index of the fiber, and $A_{\rm eff}$ is the effective optical mode cross sectional area. The MZM transfer function can be written as

$$\begin{bmatrix} E_{\rm out1}(t) \\ E_{\rm out2}(t) \end{bmatrix} = \frac{1}{2}\begin{bmatrix} 1 & i \\ i & 1 \end{bmatrix}\begin{bmatrix} e^{i\phi_1(t)} & 0 \\ 0 & e^{i\phi_2(t)} \end{bmatrix} \times \begin{bmatrix} 1 & i \\ i & 1 \end{bmatrix}\begin{bmatrix} E_{\rm in}(t) \\ 0 \end{bmatrix} \tag{1}$$

where

$$\phi_1(t) = \begin{cases} \phi_{\rm dc1} + \frac{\phi_{rf1}}{\sqrt{2}}\sin(\Omega_{rf}t), & 90^\circ \text{ Hybrid} \\ & \text{and } 180^\circ \text{ Hybrid} \\ \phi_{\rm dc1} + \phi_{rf1}\sin(\Omega_{rf}t), & 50\,\Omega \text{ Load} \end{cases} \tag{2}$$

and

$$\phi_2(t) = \begin{cases} \phi_{\rm dc2} + \frac{\phi_{rf2}}{\sqrt{2}}\cos(\Omega_{rf}t), & 90^\circ \text{ Hybrid} \\ \phi_{\rm dc2} - \frac{\phi_{rf2}}{\sqrt{2}}\sin(\Omega_{rf}t), & 180^\circ \text{ Hybrid} \\ 0, \quad 50\,\Omega \text{ Load} \end{cases} \tag{3}$$

depending on what configuration is chosen in Fig. 1. Note $\phi_{\rm dc1,2} = \pi(V_{\rm dc1,2}/V_{\pi,\rm dc1,2})$ and $\phi_{rf1,2} = \pi(V_{rf1,2}/V_{\pi,rf1,2}(\Omega_{rf}))$, where $V_{\pi,\rm dc}$ is the externally applied dc voltage required to move the optical output of the MZM from a minimum to a maximum and $V_{\pi,rf}(\Omega_{rf})$ is the externally applied RF voltage required to move the optical output of the MZM from a minimum to a maximum at an RF angular frequency $\Omega_{\rm rf}$. The modulation index of the MZM, commonly denoted as m [12], can be derived in our notation by the relation $m_{1,2} = \phi_{rf1,2}/\pi$. In order to generate SSB modulation, the 90° hybrid is used and we will follow this math to determine the RF gain and the two-tone output intercept point. The math for the other two cases requires replacing ϕ_2(t) with the proper definition. We will provide the results of this analysis when we compare the SSB case with the two other DSB cases.

Choosing one of the outputs of the MZM transfer function, the total output field of the MZM is given by

$$E_{\rm out}(t) = \frac{1}{2}\left(e^{i\phi_1(t)} - e^{i\phi_2(t)}\right)E_{\rm in}(t). \tag{4}$$

For this treatment, we are going to focus on the carrier and the first upper and lower side bands. We also assume the same RF signal onto both arms of the MZM so $\phi_{rf1} = \phi_{rf2}$. Rewriting (4) with the definitions of ϕ_1(t) and ϕ_2(t) as given above and making use of the Jacobi Anger expansions, the field for the carrier and fundamental RF sidebands can be written as

$$E_{\rm carrier}(t) = \frac{\bar{E}_{\rm in}e^{i\omega_o t}}{2}J_0\left(\frac{\phi_{rf}}{\sqrt{2}}\right)\left[e^{i\phi_{\rm dc1}} - e^{i\phi_{\rm dc2}}\right] \tag{5a}$$

$$E_{\rm usb,fund}(t) = \frac{\bar{E}_{\rm in}e^{i(\omega_o-\Omega_{rf})t}}{2}J_1\left(\frac{\phi_{rf}}{\sqrt{2}}\right)\left[-e^{i\phi_{\rm dc1}} - ie^{i\phi_{\rm dc2}}\right]$$

$$E_{\rm lsb,fund}(t) = \frac{\bar{E}_{\rm in}e^{i(\omega_o+\Omega_{rf})t}}{2}J_1\left(\frac{\phi_{rf}}{\sqrt{2}}\right)\left[e^{i\phi_{\rm dc1}} - ie^{i\phi_{\rm dc2}}\right] \tag{5b}$$

where $J_{\rm n}$ is the nth-order Bessel function and $E_{\rm in}(t) = \bar{E}_{\rm in}e^{i\omega_o t}$. By inspection of (see 5b), the upper fundamental optical sideband is nulled when $\phi_{\rm dc1} = -\pi/2 + \phi_{\rm dc2}$, and the lower fundamental sideband is nulled when $\phi_{\rm dc1} = \pi/2 + \phi_{\rm dc2}$. The fields for the 180° hybrid and the single arm case can also be derived using the methods above and will yield the following for the 180° hybrid

$$E_{\rm carrier}(t) = \frac{\bar{E}_{\rm in}e^{i\omega_o t}}{2}J_0\left(\frac{\phi_{rf}}{\sqrt{2}}\right)\left[e^{i\phi_{\rm dc1}} - e^{i\phi_{\rm dc2}}\right] \tag{6a}$$

$$E_{\mathrm{usb,fund}}(t) = \frac{\bar{E}_{\mathrm{in}} e^{i(\omega_o - \Omega_{rf})t}}{2} J_1\left(\frac{\phi_{rf}}{\sqrt{2}}\right)\left[-e^{i\phi_{\mathrm{dc1}}} - e^{i\phi_{\mathrm{dc2}}}\right]$$

$$E_{\mathrm{lsb,fund}}(t) = \frac{\bar{E}_{\mathrm{in}} e^{i(\omega_o + \Omega_{rf})t}}{2} J_1\left(\frac{\phi_{rf}}{\sqrt{2}}\right)\left[e^{i\phi_{\mathrm{dc1}}} + e^{i\phi_{\mathrm{dc2}}}\right] \quad (6b)$$

and the following for the single arm case

$$E_{\mathrm{carrier}}(t) = \frac{\bar{E}_{\mathrm{in}} e^{i\omega_o t}}{2}\left[e^{i\phi_{\mathrm{dc1}}} J_0(\phi_{rf}) - 1\right] \quad (7a)$$

$$E_{\mathrm{usb,fund}}(t) = \frac{\bar{E}_{\mathrm{in}} e^{i(\omega_o - \Omega_{rf})t}}{2}\left[-e^{i\phi_{\mathrm{dc1}}} J_1(\phi_{rf})\right]$$

$$E_{\mathrm{lsb,fund}}(t) = \frac{\bar{E}_{\mathrm{in}} e^{i(\omega_o + \Omega_{rf})t}}{2}\left[e^{i\phi_{\mathrm{dc1}}} J_1(\phi_{rf})\right]. \quad (7b)$$

With the carrier and fundamental fields now derived, the optical power can be calculated in order to compare the power of the SSB carrier and sidebands with those of the DSB cases. The average optical powers of the carrier, upper and lower sidebands are related to the field amplitudes by $E^*_{\mathrm{carrier,usb,lsb}} E_{\mathrm{carrier,usb,lsb}} = 2\kappa^2_{\mathrm{carrier,usb,lsb}} P_{o,\mathrm{carrier,usb,lsb}}$, respectively, with κ^2 defined the same as above. The HR-OSA will then be used to validate the theoretical predictions. Starting with the SSB case (see 5a) and (see 5b) and using the small signal approximation of $J_n(\phi_{rf}) \approx \phi^n_{rf}/(2^n n!)$, the optical power of the carrier and each of the sidebands is given by

$$P_{o,\mathrm{carrier}} \approx \gamma_{\mathrm{carrier}} \frac{P_{\mathrm{laser}}}{4}\left[2 - 2\cos(\phi_{\mathrm{dc1}} - \phi_{\mathrm{dc2}})\right] \quad (8a)$$

$$P_{o,\mathrm{usb,fund}} \approx \gamma_{\mathrm{usb}} \frac{P_{\mathrm{laser}}}{32}\phi^2_{rf}\left[2 + 2\sin(\phi_{\mathrm{dc1}} - \phi_{\mathrm{dc2}})\right]$$

$$P_{o,\mathrm{lsb,fund}} \approx \gamma_{\mathrm{lsb}} \frac{P_{\mathrm{laser}}}{32}\phi^2_{rf}\left[2 - 2\sin(\phi_{\mathrm{dc1}} - \phi_{\mathrm{dc2}})\right] \quad (8b)$$

where $\gamma_{\mathrm{carrier,usb,lsb}} = \kappa^2_{\mathrm{laser}}/\kappa^2_{\mathrm{carrier,usb,lsb}}$. Similarly the optical power can be derived for the 180° hybrid

$$P_{o,\mathrm{carrier}} \approx \gamma_{\mathrm{carrier}} \frac{P_{\mathrm{laser}}}{4}\left[2 - 2\cos(\phi_{\mathrm{dc1}} - \phi_{\mathrm{dc2}})\right] \quad (9a)$$

$$P_{o,\mathrm{usb,fund}} \approx \gamma_{\mathrm{usb}} \frac{P_{\mathrm{laser}}}{32}\phi^2_{rf}\left[2 + 2\cos(\phi_{\mathrm{dc1}} - \phi_{\mathrm{dc2}})\right]$$

$$P_{o,\mathrm{lsb,fund}} \approx \gamma_{\mathrm{lsb}} \frac{P_{\mathrm{laser}}}{32}\phi^2_{rf}\left[2 + 2\cos(\phi_{\mathrm{dc1}} - \phi_{\mathrm{dc2}})\right] \quad (9b)$$

and the single arm drive

$$P_{o,\mathrm{carrier}} \approx \gamma_{\mathrm{carrier}} \frac{P_{\mathrm{laser}}}{4}\left[2 - \cos(\phi_{\mathrm{dc1}})\right] \quad (10a)$$

$$P_{o,\mathrm{usb,fund}} \approx \gamma_{\mathrm{usb}} \frac{P_{\mathrm{laser}}}{16}\phi^2_{rf}$$

$$P_{o,\mathrm{lsb,fund}} \approx \gamma_{\mathrm{lsb}} \frac{P_{\mathrm{laser}}}{16}\phi^2_{rf}. \quad (10b)$$

From (8)–(10), the optical power at the carrier is the same in all three cases if the quadrature bias condition ($\phi_{\mathrm{dc1}} = -\pi/2 + \phi_{\mathrm{dc2}}$ or $\phi_{\mathrm{dc1}} = \pi/2 + \phi_{\mathrm{dc2}}$, with $\phi_{\mathrm{dc2}} = 0$ for the single arm) is chosen. The optical sidebands of the single arm and 180° hybrid are the same. For the 90° hybrid case, the SSB of the 90° hybrid is 3 dB higher than both of the DSB cases. We experimentally confirm these results for the three cases by measuring the optical spectrum on the HR-OSA. The HR-OSA has sufficient resolution to clearly show the 5 GHz sidebands, which is not observable with a typical OSA. The results are shown in Fig. 2 for a 5 GHz RF input tone. The modulation index, *m*, is 7.5% for all three cases. We used the same input RF power and the RF V_π (2.1 V at 5 GHz) is the same in all three cases since it is the same MZM. We chose this modulation index for two reasons. First, analog photonic links mostly use small signal modulation to avoid unwanted nonlinear effects due to the sinusoidal transfer function of the MZM [20]. Second, the theoretical analysis uses the small signal approximation for the Bessel functions to write the analytic equations. So we hold the RF input power much less than the RF V_π to keep our assumptions true. When the MZM is set to SSB modulation with the 90° hybrid, the sideband (−21.3 dBm) is approximately 3 dB higher than either the DSB from the 180° hybrid (−24.1 dBm) or the single arm case (−24.4 dBm). The suppressed sideband of the 90° hybrid case is extinguished by over 40 dB when compared to the DSB cases. The extinction ratio is limited to this range by the non-ideal phase performance of the 90° hybrid, as well as the slight mismatch in the physical length of RF cables that connect the 90° hybrid to the RF ports of the MZM. In this case we expect the RF output power from the 180° hybrid and the single arm case to be 3 dB higher than the SSB case of the 90° hybrid. However this is not the case for the single arm and will be shown in the following section. Note the smaller sidebands are inherent to the HR-OSA (APEX AP2040 series) measurement system and are from neither the RF signal nor the MZM link and the upper sidebands are shifted slightly in order to see the difference between the three cases.

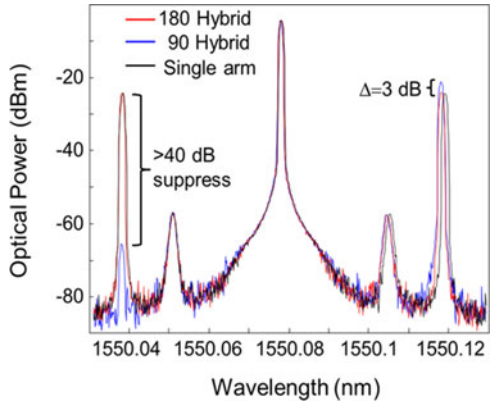

Fig. 2. Measured optical spectra of the 90° hybrid, 180° hybrid and single arm configurations. The 90° hybrid suppresses the lower sideband by over 40 dB while providing 3 dB higher optical power than the 180° hybrid and the single arm cases. Note the smaller sidebands are inherent to the HR-OSA system (APEX AP2040 series) and are not from the RF signal. Also the upper sidebands are shifted slightly to see the difference between the three cases.

As an additional comparison, we can write the optical power of the carrier and DSBs from an X-cut $LiNbO_3$ MZM that provides an internal push-pull configuration with a single RF input.

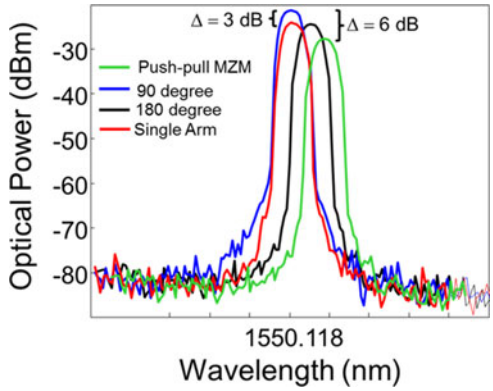

Fig. 3. Simulated optical sidebands of the 90° hybrid, 180° hybrid, push-pull and single arm configurations. The 90° hybrid provides 3 dB higher optical power than either the 180° hybrid or the single arm case. It is 6 dB higher than the push-pull configuration.

By the placement of the electrodes in an X-cut MZM, the RF drive voltage is split evenly across the two optical waveguides, creating an inherent push-pull modulation [21]. This inherent push-pull requires no external hybrid, making the devices easier to work with at a system level. However the trade-off with working with X-cut MZMs is they often have higher RF V_π due to the lower overlap of the electric fields in the optical waveguide [20], [21]. For this analysis, we will assume an X-cut MZM which has the same RF V_π, DC V_π, and insertion loss as the Z-cut MZM that we are using. We will also assume the same optical power from the laser. Under these conditions, the push-pull MZM will have the same ϕ_{rf}, $\phi_{\rm dc}$, $P_{\rm laser}$ and γ as we use in our analysis. Given this assumption, the transfer function of the push-pull MZMs have been well studied in the literature [9] and we will compare the powers predicted theoretically. We will not compare the push-pull MZM experimentally since we have no modulators with exactly the same $V_{\pi,\rm dc}$ or $V_{\pi,rf}$ as the Z-cut MZM we are using. Nevertheless the theory is enough to compare. The push-pull MZM optical carrier and sideband powers are given by [9]

$$P_{o,\rm carrier} \approx \gamma_{\rm carrier}\frac{P_{\rm laser}}{4}\left[2-2\cos(\phi_{\rm dc1})\right] \quad (11a)$$

$$P_{o,\rm usb,fund} \approx \gamma_{\rm usb}\frac{P_{\rm laser}}{64}\phi_{rf}^2\left[2+2\cos(\phi_{\rm dc1})\right]$$

$$P_{o,\rm lsb,fund} \approx \gamma_{\rm lsb}\frac{P_{\rm laser}}{64}\phi_{rf}^2\left[2+2\cos(\phi_{\rm dc1})\right]. \quad (11b)$$

From these results, the optical carrier is the same as all the other cases when the quadrature bias condition is chosen ($\phi_{\rm dc1}=\pm\pi/2$). However the optical DSBs of the push-pull MZM are 3 dB less than the 180° hybrid and single arm DSBs and 6 dB less than the 90° hybrid SSB. These results are shown in Fig. 3. The sidebands are simulated for the four different modulation types with all the same parameters as in the experimentally measured case in Fig. 2. Another way that the X-cut MZM and the Z-cut single arm MZM are different is shown in Eqns. (10b) and (11b). The optical sideband powers for a Z-cut MZM have no dependence on $\phi_{\rm dc1}$, while the X-cut MZM optical sidebands do. If one observes the sidebands on an OSA and then changes the dc bias applied to the MZM, the optical sidebands will change power if the MZM is an X-cut but they will remain unchanged if it is a Z-cut. This is a relatively simple method to differentiate between the two MZMs. The RF output power for all of these cases will now be described and measured in the next section.

III. Theory and Experiment of RF Output Power of the SSB and DSB Link

In order to calculate the RF output power of the SSB and DSB link, the total optical power from the MZM must be derived. Taking the field in Eqn. (4) and multiplying by its complex conjugate to get the optical power from the MZM yields

$$P_{o,\rm MZM}(t)=\frac{\alpha_{\rm MZM}P_{\rm laser}}{4}\left[2-2\cos(\phi_1(t)-\phi_2(t))\right] \quad (12)$$

where $\alpha_{\rm MZM}$ is the optical insertion loss for the MZM. Expanding $\phi_{1,2}(t)$ in (12) for the SSB case yields

$$P_{o,\rm MZM,SSB}(t)=\frac{\alpha_{\rm MZM}P_{\rm laser}}{4}\times\begin{bmatrix}2-2\cos(\Delta\phi_{\rm dc})\cos\left[\phi_{rf}\sin\left(\Omega_{rf}t-\frac{\pi}{4}\right)\right]\\+2\sin(\Delta\phi_{\rm dc})\sin\left[\phi_{rf}\sin\left(\Omega_{rf}t-\frac{\pi}{4}\right)\right]\end{bmatrix} \quad (13)$$

with $\Delta\phi_{\rm dc}=\phi_{\rm dc1}-\phi_{\rm dc2}$. Replacing the RF terms with their equivalent infinite sums of Bessel functions and regrouping for dc, fundamental (odd) and second (even) harmonic power, the following can be written

$$P_{o,\rm MZM,SSB}(t)=\frac{\alpha_{\rm MZM}P_{\rm laser}}{2}\times\begin{bmatrix}1-\cos(\Delta\phi_{\rm DC})J_0(\phi_{rf})\,[\rm DC]\\+2\sin(\Delta\phi_{\rm dc})\sum_{n=1}^{\infty}J_{2n-1}(\phi_{rf})\sin\begin{pmatrix}(2n-1)\Omega_{rf}t\\-(2n-1)\frac{\pi}{4}\end{pmatrix}[\rm odd]\\-2\cos(\Delta\phi_{\rm dc})\sum_{n=1}^{\infty}J_{2n}(\phi_{rf})\cos\begin{pmatrix}2n\Omega_{rf}t\\-2n\frac{\pi}{4}\end{pmatrix}[\rm even]\end{bmatrix}. \quad (14)$$

Equation (14) shows that when the SSB condition is met (either $\phi_{\rm dc1}=\pi/2+\phi_{\rm dc2}$ or $\phi_{\rm dc1}=-\pi/2+\phi_{\rm dc2}$), the even order harmonics are nulled, thus preserving the quadrature operation of DSB modulation. The fundamental RF power can now be derived. The generated photocurrent due to the optical power can be written as

$$I_{\rm Fund,MZM,SSB}(t)=\Re\alpha_{\rm MZM}P_{\rm laser}\sin(\Delta\phi_{\rm dc})J_1(\phi_{rf})\times\sin\left(\Omega_{rf}t-\frac{\pi}{4}\right) \quad (15)$$

where $\Re$ is the PD responsivity. Finally, applying the small signal approximation of $J_n(\phi_{rf})\approx\phi_{rf}^n/(2^n n!)$, the RF output power can be written as

$$P_{RF,{\rm Fund},ss}\approx(\Re\alpha_{\rm MZM}P_{\rm laser})^2\sin^2(\Delta\phi_{\rm dc})\frac{\phi_{rf}^2}{8}Z_{\rm out} \quad (16)$$

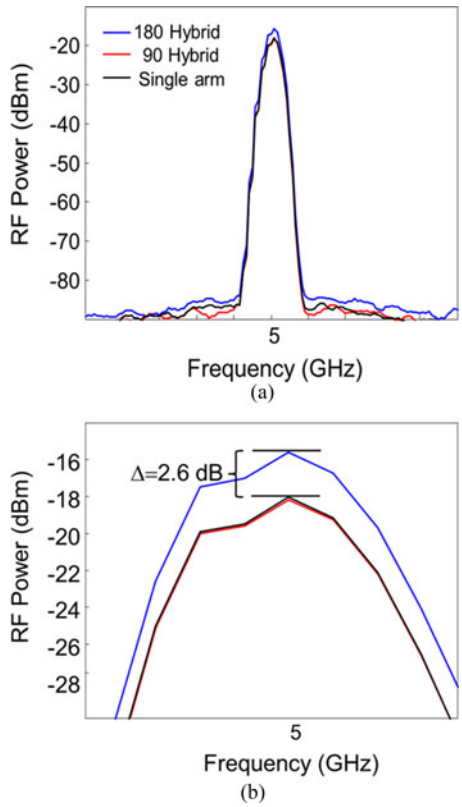

Fig. 4. (a) Measured RF powers of 5 GHz tone of the 90° hybrid, 180° hybrid and single arm configurations. (b) Magnified view of the peak signal of all three conditions showing the 180° hybrid has 2.6 dB higher power than either the 90° hybrid or the single arm case.

where $Z_{\rm out}$ is the output impedance. Note the output power is maximized when the DC bias is set to the SSB condition. In order to compare SSB with DSB, we look at the RF power for both the 180° hybrid and the single arm case. Repeating the math shown above for those conditions yields the RF output power for the 180° hybrid as

$$P_{RF,\mathrm{Fund},ss} \approx (\Re\alpha_{\rm MZM} P_{\rm laser})^2 \sin^2(\Delta\phi_{\rm dc}) \frac{\phi_{rf}^2}{4} Z_{\rm out} \quad (17)$$

and for the single arm case

$$P_{RF,\mathrm{Fund},ss} \approx (\Re\alpha_{\rm MZM} P_{\rm laser})^2 \sin^2(\phi_{\rm dc1}) \frac{\phi_{rf}^2}{8} Z_{\rm out}. \quad (18)$$

Note the RF power is 3 dB higher than the SSB case for the 180° hybrid case and the same for the single arm case. In order to validate this result, the RF output power from the link in Fig. 1 is measured with the same input RF power for all three configurations. The measured power is shown in Fig. 4 at the same photocurrent from the photodetector. Again in this case, the modulation index is 7.5% for all three cases. The modulation index was chosen for the same reasons as given in the previous section. The results show that the RF output power is indeed the same for both the SSB (-18.3 dBm) and the single arm DSB (-18.2 dBm) case. In addition, the 180° hybrid DSB is 2.6 dB higher (-15.6 dBm), which is within the measurement error for the system. From the optical spectrum results in the previous section, the prediction would have been that the single arm case would also have been 3 dB higher. However this points out that the optical spectrum does not always accurately predict the RF response. Due to the asymmetry in the RF drive of the single arm MZM, the unmodulated optical carrier does not contribute to the RF output power at the photodetector. This explains how the SSB and the single arm DSB have the same output power.

Again the RF output power of a push-pull MZM DSB link can be compared theoretically. Making the same assumptions about the push-pull MZM as in the previous section (same ϕ_{rf}, $\phi_{\rm dc}$, $P_{\rm laser}$ and $\alpha_{\rm MZM}$), the output RF power is [9]

$$P_{RF,\mathrm{Fund},ss} \approx (\Re\alpha_{\rm MZM} P_{\rm laser})^2 \sin^2(\phi_{\rm dc1}) \frac{\phi_{rf}^2}{8} Z_{\rm out}. \quad (19)$$

As predicted by the optical DSBs and carrier power in the previous section, the RF output power is the same as the SSB case and also for the single arm DSB case. These results show that the SSB link will provide the same RF output power as the DSB link using either a single arm MZM or push-pull MZM.

IV. Theory and Experiment of Third Order Intermodulation Distortion With SSB and DSB Modulation

Beyond the output RF power, the third order nonlinear response is also important in RF links using MZMs. We have already shown that the SSB MZM will not add any even order distortions, just as the push-pull MZM does not. The derivation of the output intercept point for the third order distortions is shown and verified with experiment.

In order to look at the intermodulation distortion of SSB modulation, two RF signals are input to the MZM. The signals are represented by $\phi_1(t) = \phi_{\rm dc1} + \frac{\phi_{rf1}}{\sqrt{2}} \sin\Omega_{rf1}t + \frac{\phi_{\rm rf2}}{\sqrt{2}} \sin\Omega_{rf2}t$ and $\phi_2(t) = \phi_{\rm dc2} + \frac{\phi_{rf1}}{\sqrt{2}} \cos\Omega_{rf1}t + \frac{\phi_{rf2}}{\sqrt{2}} \cos\Omega_{rf2}t$. Following the optical power function give in (12) and rearranging terms, the following can be written

$$P_{o,\mathrm{MZM,SSB}}(t) = \frac{\alpha_{\rm MZM} P_{\rm laser}}{4} \times$$

$$\left[2 - 2\left[\cos(\Delta\phi_{\rm dc}) \begin{bmatrix} \cos\left(\phi_{rf1}\sin\left(\Omega_{rf1}t - \frac{\pi}{4}\right)\right) \\ \cos\left(\phi_{rf2}\sin\left(\Omega_{rf2}t - \frac{\pi}{4}\right)\right) \\ -\sin\left(\phi_{rf1}\sin\left(\Omega_{rf1}t - \frac{\pi}{4}\right)\right) \\ \sin\left(\phi_{rf2}\sin\left(\Omega_{rf2}t - \frac{\pi}{4}\right)\right) \end{bmatrix}\right.\right.$$

$$\left.\left. - \sin(\Delta\phi_{\rm dc}) \begin{bmatrix} \sin\left(\phi_{rf1}\sin\left(\Omega_{rf1}t - \frac{\pi}{4}\right)\right) \\ \cos\left(\phi_{rf2}\sin\left(\Omega_{rf2}t - \frac{\pi}{4}\right)\right) \\ +\cos\left(\phi_{rf1}\sin\left(\Omega_{rf1}t - \frac{\pi}{4}\right)\right) \\ \sin\left(\phi_{rf2}\sin\left(\Omega_{rf2}t - \frac{\pi}{4}\right)\right) \end{bmatrix}\right]\right]. \quad (20)$$

Replacing the RF terms with their equivalent infinite sums of Bessel functions and regrouping for odd frequency components of the optical power, as shwon at the bottom of the page.

From the equations (20) and (21), one can find the output intercept points for the third order intermodulation distortion. For the third order, setting $\phi_{rf1} = \phi_{rf2}$ and using the small signal approximation for the Bessel function the RF power for the $2\Omega_{rf2} - \Omega_{rf1}$ term can be written as

$$P_{RF,\mathrm{SSB},2\Omega_{rf2}-\Omega_{rf1},ss} \approx (\Re\alpha_{\mathrm{MZM}} P_{\mathrm{laser}})^2 \times \sin^2(\Delta\phi_{\mathrm{dc}}) \frac{\phi_{rf}^6}{512} Z_{\mathrm{out}} \quad (22)$$

and the RF power of the signal at Ω_{rf2} is

$$P_{RF,\mathrm{SSB},\Omega_{rf2},ss} \approx (\Re\alpha_{\mathrm{MZM}} P_{\mathrm{laser}})^2 \sin^2(\Delta\phi_{\mathrm{dc}}) \frac{\phi_{rf}^2}{8} Z_{\mathrm{out}}. \quad (23)$$

Setting (22) and (23) equal to each other, solving for ϕ_{rf}, and then plugging the result back into (23) yields

$$OIP3_{imd,\mathrm{SSB}} = (\Re\alpha_{\mathrm{MZM}} P_{\mathrm{laser}})^2 \sin^2(\Delta\phi_{\mathrm{dc}}) Z_{\mathrm{out}}. \quad (24)$$

Using the same derivation, the 180° hybrid has an RF power for the $2\Omega_{rf2} - \Omega_{rf1}$ third order intermodulation power of

$$P_{RF,\mathrm{DSB},2\Omega_{rf2}-\Omega_{rf1},ss} \approx (\Re\alpha_{\mathrm{MZM}} P_{\mathrm{laser}})^2 \times \sin^2(\Delta\phi_{\mathrm{dc}}) \frac{\phi_{rf}^6}{64} Z_{\mathrm{out}} \quad (25)$$

and an RF output power at Ω_{rf2} of

$$P_{RF,\mathrm{DSB},\Omega_{rf2},ss} \approx (\Re\alpha_{\mathrm{MZM}} P_{\mathrm{laser}})^2 \sin^2(\Delta\phi_{\mathrm{dc}}) \frac{\phi_{rf}^2}{4} Z_{\mathrm{out}} \quad (26)$$

yielding an $\mathrm{OIP3}_{\mathrm{imd}}$ of

$$OIP3_{imd,\mathrm{DSB}} = (\Re\alpha_{\mathrm{MZM}} P_{\mathrm{laser}})^2 \sin^2(\Delta\phi_{\mathrm{dc}}) Z_{\mathrm{out}}. \quad (27)$$

For the single arm MZM, the RF power for the $2\Omega_{rf2} - \Omega_{rf1}$ third order intermodulation power and RF power for the Ω_{rf2} are the same as the SSB case and thus the $\mathrm{OIP3}_{\mathrm{imd}}$ is also the same.

This was experimentally measured and the results appear in Fig. 5(a)–(c). In this instance, the single arm (1.32 dBm), 180° (1.85 dBm) and 90° hybrid (1.12 dBm) case have the same OIP3 value within the error of measurement. Note that the measurement was made at a photocurrent of 5.3 mA which predicts an $\mathrm{OIP3}_{\mathrm{imd}}$ of 1.48 dBm, accounting for the 50 Ω termination at the RF output of the photodetector [9]. The simulated results of the push-pull MZM are also presented in Fig. 5(d) with an extrapolated $\mathrm{OIP3}_{\mathrm{imd}}$ of 1.48 dBm. We also note the noise floor of the link is −162 dBm/Hz in all the cases and the third order intermodulation spur free dynamic range ($\mathrm{SFDR3}_{\mathrm{imd}}$) vary from 108.7 dB · $\mathrm{Hz}^{2/3}$ (90° hybrid), 108.9 dB · $\mathrm{Hz}^{2/3}$ (single arm), 109 dB · $\mathrm{Hz}^{2/3}$ (push-pull) and 109.2 dB · $\mathrm{Hz}^{2/3}$ (180° hybrid). For the laser RIN limited noise floor and the 5.3 mA photocurrent, an SFDR3 around 109 dB · $\mathrm{Hz}^{2/3}$ is consistent with the theory Ref. [9, Fig. 12(b)]. This is consistent with the measurement that was made. This demonstrates that the 90° hybrid for SSB operation has the same RF output power and third order intermodulation performance as the single arm DSB modulation.

As with the RF output power, the push-pull MZM will also have the same $\mathrm{OIP3}_{\mathrm{imd}}$ performance as the single arm driven MZM [9]. The simulated results are shown in Fig 5(d). Thus SSB modulation can provide the same RF performance in both power and intermodulation distortion as the DSB modulation from a push-pull MZM.

V. Conclusion

SSB optical modulation offers advantages in RF fading and compensating nonlinear performance of photodetectors over DSB optical techniques in photonic links. However the SSB RF link is still limited to niche applications and has not been widely adopted. One of the reasons comes from a lack of a detailed analysis of the SSB link's RF output power and nonlinear performance as compared to DSB links. Starting with the first

$$P_{o,\mathrm{MZM,SSB}}(t) = \alpha_{\mathrm{MZM}} P_{\mathrm{laser}} \sin(\Delta\phi_{\mathrm{dc}}) \left[\begin{array}{l} J_0(\phi_{rf2}) \sum_{n=1}^{\infty} J_{2n-1}(\phi_{rf1}) \sin\left((2n-1)\Omega_{rf1}t - (2n-1)\frac{\pi}{4}\right) \\ +J_0(\phi_{rf1}) \sum_{n=1}^{\infty} J_{2n-1}(\phi_{rf2}) \sin\left((2n-1)\Omega_{rf2}t - (2n-1)\frac{\pi}{4}\right) \\ -\sum_{n=1}^{\infty}\sum_{k=1}^{\infty} J_{2n-1}(\phi_{rf1}) J_{2k}(\phi_{rf2}) \sin\left(\begin{array}{l}(2k\Omega_{rf2} - (2n-1)\,\Omega_{rf1})t \\ -(2k-(2n-1))\frac{\pi}{4}\end{array}\right) \\ -\sum_{n=1}^{\infty}\sum_{k=1}^{\infty} J_{2n-1}(\phi_{rf2}) J_{2k}(\phi_{rf1}) \sin\left(\begin{array}{l}(2k\Omega_{rf1} - (2n-1)\,\Omega_{rf2})t \\ -(2k-(2n-1))\frac{\pi}{4}\end{array}\right) \\ +\sum_{n=1}^{\infty}\sum_{k=1}^{\infty} J_{2n-1}(\phi_{rf1}) J_{2k}(\phi_{rf2}) \sin\left(\begin{array}{l}(2k\Omega_{rf2} + (2n-1)\,\Omega_{rf1})t \\ -(2k+(2n-1))\frac{\pi}{4}\end{array}\right) \\ +\sum_{n=1}^{\infty}\sum_{k=1}^{\infty} J_{2n-1}(\phi_{rf2}) J_{2k}(\phi_{rf1}) \sin\left(\begin{array}{l}(2k\Omega_{rf1} + (2n-1)\,\Omega_{rf2})t \\ -(2k+(2n-1))\frac{\pi}{4}\end{array}\right) \end{array} \right]. \quad (21)$$

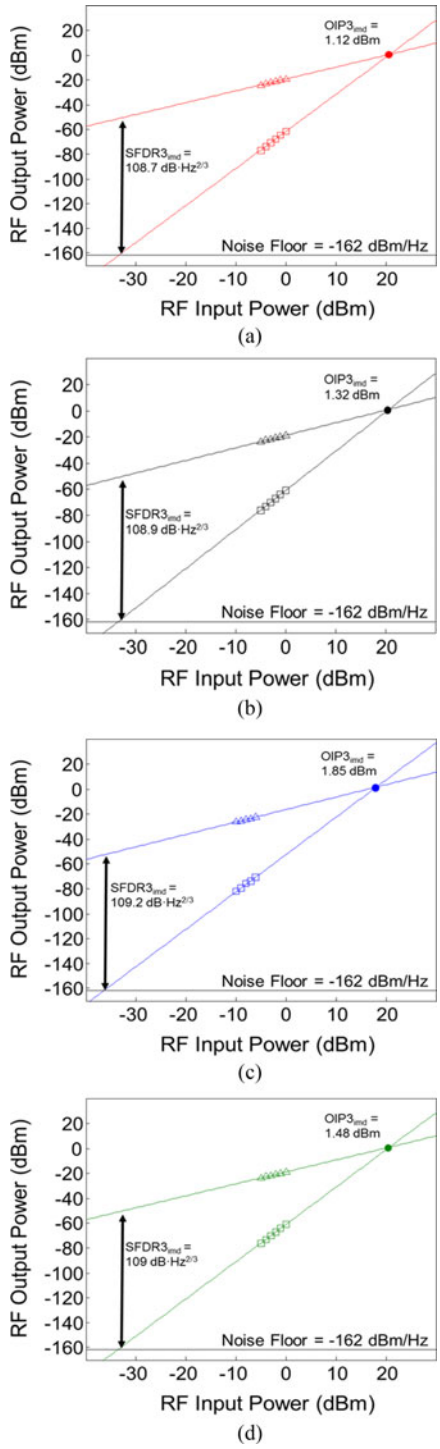

Fig. 5. Measured RF powers of fundamental and third order intermodulation distortion for two input tones of 5 and 5.1 GHz of (a) 90° hybrid, (b) single arm and (c) 180° hybrid case. The simulated RF powers of a push-pull MZM appear in (d). The extrapolated $\mathrm{OIP3_{imd}}$ and $\mathrm{SFDR3_{imd}}$ is the same for all four cases.

principles of the MZM transfer function, analytic expressions are derived for the optical sideband power, RF output power and the third order intermodulation nonlinearity for the SSB case as well as three other DSB cases. The predicted performance from the analytic expressions is then measured experimentally to validate the theory. We have demonstrated that SSB optical modulation can be used in these photonic links without any sacrifice to the RF performance when compared to either a single arm MZM providing DSB modulation or a push-pull X-cut MZM that has the same operating parameters (insertion loss and V_π) as the Z-cut MZM. As seen in Table I, the SSB modulation from a 90° hybrid MZM has the same OIP3 performance as the three other cases. While the SSB link does provide 3 dB less RF output power when compared to a DSB link using a 180 hybrid, the SSB link has the same RF output power as the push-pull X-cut MZM and the single arm MZM links. The SSB modulation increases the optical power in the sideband that is not nulled, thus making up for the loss of the other sideband, which is a non-intuitive result and has to be mathematically derived and experimentally demonstrated. We have made both theoretical and experimental measurements in order to verify the performance of the SSB modulation when compared to the DSB modulation of the single arm driven MZM and the 180° hybrid. While the OSA measurement of the DSB with a single arm driven MZM is only 3 dB lower, the RF output power is the same. The OSA does not measure phase between the two sidebands and the unmodulated optical carrier in the single arm case is enough to cause the RF power after photodetection to be equal to the SSB case. Again this is a non-intuitive result given how the other modulation formats RF output power relates to the relative optical power of the sidebands. The push-pull MZM has been modeled extensively [9] and those results are used to show a push-pull MZM has 6 dB lower sidebands mathematically and has the same output RF power and $\mathrm{OIP3_{imd}}$ as the SSB case, assuming the same V_π and insertion loss. This paper provides a complete analysis of the optical sideband performance as well as the RF performance of not only a SSB modulated link but three other DSB modulated links, allowing an RF photonic link designer the tools needed to decide which type of link to use.

TABLE I
COMPARISON OF SIDEBAND OPTICAL POWER, RF OUTPUT POWER AND OIP3 RELATIVE TO SSB MODULATION FOR THREE DIFFERENT CASES

	Optical Sideband Power relative to SSB (dB)	RF Output power relative to SSB (dB)	$\mathrm{OIP3_{imd}}$ relative to SSB (dB)
180 Hybrid (DSB)	−3	+3	0
Push-pull X-cut (DSB)	−6	0	0
Single Arm (DSB)	−3	0	0
90 Hybrid (SSB)	0	0	0

REFERENCES

[1] J. E. Roman, L. T. Nichols, K. J. Williams, R. D. Esman, G. C. Tavik, M. Livingston, and M. G. Parent, "Fiber-optic remoting of an ultrahigh dynamic range radar," *IEEE Trans. Microw. Theory Tech.*, vol. 46, no. 12, pp. 2317–2323, Dec. 1998.

[2] C. Chang, J. A. Cassaboom, and H. F. Taylor, "Fiber optic delay line devices for RF signal processing," *Electron. Lett.*, vol. 13, pp. 678–680, 1977.

[3] S. Pan and J. Yao, "Optical clock recovery using a polarization-modulator-based frequency-doubling optoelectronic oscillator," *J. Lightw. Technol.*, vol. 27, no. 16, pp. 3531–3539, Aug. 2009.

[4] H. Tsuchida and M. Suzuki, "40-Gb/s optical clock recovery using an injection-locked optoelectronic oscillator," *IEEE Photon. Technol. Lett.*, vol. 17, no. 1, pp. 211–213, Jan. 2005.
[5] W. Zhou and G. Blasche, "Injection-locked dual opto-electronic oscillator with ultra-low phase noise and ultra-low spurious level," *IEEE Trans. Microw. Theory Tech.*, vol. 53, pp. 929–932, 2005.
[6] P. S. Devgan, V. J. Urick, J. F. Diehl, and K. J. Williams, "Improvement in the phase noise of a 10 GHz optoelectronic oscillator using all-photonic gain," *J. Lightw. Technol.*, vol. 27, no. 15, pp. 3189–3193, Aug. 2009.
[7] P. Devgan, M. Pruessner, V. Urick, and K. Williams, "Detecting low-power RF signals using a multimode optoelectronic oscillator and integrated optical filter," *IEEE Photon. Technol. Lett.*, vol. 22, no. 3, pp. 152–154, Feb. 2010.
[8] P. Devgan, V. Urick, and K. Williams, "Detection of low-power RF signals using a two laser multimode optoelectronic oscillator," *IEEE Photon. Technol. Lett.*, vol. 24, no. 10, pp. 857–859, May 2012.
[9] V. J. Urick, F. Bucholtz, J. D. McKinney, P. S. Devgan, A. L. Campillo, J. L. Dexter, and K. J. Williams, "Long-haul analog photonics," *J. Lightw. Technol.*, vol. 29, no. 8, pp. 1182–1205, Apr. 2011.
[10] H. Schmuck, "Comparison of optical millimeter-wave system concepts with regard to chromatic dispersion," *Electron. Lett.*, vol. 31, pp. 1848–1849, 1995.
[11] G. J. Meslener, "Chromatic dispersion induced distortion of modulated monochromatic light employing direct detection," *IEEE J. Quant. Electron.*, vol. QE-20, no. 10, pp. 1208–1216, Oct. 1984.
[12] B. Hraimel, X. Zhang, Y. Pei, K. Wu, T. Liu, T. Xu, and Q. Nie, "Optical single-sideband modulation with tunable optical carrier to sideband ratio in radio over fiber systems," *J. Lightw. Technol.*, vol. 29, no. 5, pp. 775–781, Mar. 2011.
[13] J. Park, W. V. Sorin, and K. Y. Lau, "Elimination of the fiber chromatic dispersion penalty on 1550 nm millimeter-wave optical transmission," *Electron. Lett.*, vol. 33, pp. 512–513, 1997.
[14] G. H. Smith, D. Novak, and Z. Ahmed, "Technique for optical SSB generation to overcome dispersion penalties in fibre-radio systems," *Electron. Lett.*, vol. 33, pp. 74–75, 1997.
[15] A. Loayssa, D. Benito, and M. J. Garde, "Single-sideband suppressed-carrier modulation using a single-electrode electrooptic modulator," *IEEE Photon. Technol. Lett.*, vol. 13, no. 8, pp. 869–871, Aug. 2001.
[16] I. Ozdur, D. Mandridis, N. Hoghooghi, and P. Delfyett, "Low noise optically tunable opto-electronic oscillator with Fabry–Perot etalon," *J. Lightw. Technol.*, vol. 28, no. 21, pp. 3100–3106, Nov. 2010.
[17] P. S. Devgan, A. S. Hastings, V. J. Urick, and K. J. Williams, "Cancellation of photodiode-induced second harmonic distortion using single side band modulation from a dual parallel Mach-Zehnder," *Opt. Exp.*, vol. 20, pp. 27163–27173, 2012.
[18] G. Zhu, W. Liu, and H. Fetterman, "A broadband linearized coherent analog fiber-optic link employing dual parallel Mach–Zehnder modulators," *IEEE Photon. Technol. Lett.*, vol. 21, no. 21, pp. 1627–1629, Nov. 2009.
[19] C. Cox, E. Ackerman, G. Betts, and J. Prince, "Limits on the performance of RF-over-fiber links and their impact on device design," *IEEE Microw. Theory Tech.*, vol. 54, no. 2, pp. 906–920, Feb. 2006.
[20] G. Li and P. Yu, "Optical intensity modulators for digital and analog applications," *J. Lightw. Technol.*, vol. 21, no. 9, pp. 2010–2030, Sep. 2003.
[21] E. Wooten, K. Kissa, A. Yi-Yan, E. Murphy, D. Lafaw, P. Hallemeier, D. Maack, D. Attanasio, D. Fritz, G. McBrien, and D. Bossi, "A review of lithium niobate modulators for fiber-optic communications systems," *IEEE J. Sel. Topics Quantum Electron.*, vol. 6, no. 1, pp. 69–82, Jan./Feb. 2000.

Preetpaul S. Devgan (M'06–SM'13) received the B.S. degree in computer and electrical engineering and the M.S. degree in electrical engineering from Purdue University, West Lafayette, IN, USA, in 1996 and 1998, respectively. He received the Ph.D. degree in electrical engineering from Northwestern University, Evanston, IL, USA, in 2006.

From 1998 to 2001, he was with Lucent Technologies, where he was a Member of Technical Staff in the Optical Networking Group. From 2006 to 2013, he was at the Naval Research Laboratory, Washington, DC, USA, researching microwave photonic links and subsystems. He is currently working at the Air Force Research Laboratory, WPAFB, Dayton, OH, USA. His current research interests include optoelectronic oscillators for signal processing and novel modulation formats for analog links.

Dean P. Brown received the B.S. degree in engineering physics from Wright State University, Dayton, OH, USA, in 2005, and the Ph.D. degree in optics from the University of Rochester, Rochester, NY, USA, in 2010.

From 2010 to 2012, he was a Postdoctoral Research Scientist with UES, Inc., Dayton, working at the Air Force Research Laboratory. During this time, he worked on ultrafast optics, pulse shaping, nonlinear optics, and near-field microscopy. He then became a full Research Scientist and Program Manager with UES, Inc., in 2012. His current research interests include ultrafast optics, nonlinear optics, high-power fiber lasers, and RF photonic modulators and links.

Robert L. Nelson received the B.S. degree in physics from the University of Wisconsin, Eau Claire, WI, USA, in 1988, and the Ph.D. degree in optics from the University of Rochester, Rochester, NY, USA, in 1999. From 1988 to 1992, he was at Naval Nuclear Power School as an instructor, and since 1999, he is working at the Air Force Research Laboratory, Materials and Manufacturing Directorate, Dayton, OH, USA, as a Research Scientist.

His past and current research interests include composite optical materials, photonic crystals, optical and RF metamaterials, and RF photonics materials devices and systems.